Mechanical momentum transfer in wall-bounded superfluid turbulence

D. Khomenko, V. S. L'vov, A. Pomyalov, and I. Procaccia
Department of Chemical Physics, Weizmann Institute of Science, Rehovot 76100, Israel
(Received 17 December 2015; revised manuscript received 10 March 2016; published 11 April 2016)

In classical turbulence the kinematic viscosity ν is involved in two phenomena. The first is the energy dissipation and the second is the mechanical momentum flux toward the wall. In superfluid turbulence the mechanism of energy dissipation is different, and it is determined by an effective viscosity which was introduced by Vinen and is denoted as ν'. In this paper we show that in superfluid turbulence the transfer of mechanical momentum to the wall is caused by the presence of a quantum vortex tangle, giving rise to another effective "momentum" viscosity that we denote as $\nu_{\rm m}(T)$. The temperature dependence of the second effective viscosity is markedly different from Vinen's effective viscosity $\nu'(T)$. We show that the notion of vortex-tension force, playing an important role in the theory of quantum turbulence, can be understood as the gradient of the Reynolds-stress tensor, which is, in fact, determined by the second newly defined kinematic viscosity $\nu_{\rm m}(T)$.

DOI: 10.1103/PhysRevB.93.134504

I. INTRODUCTION

Below the Bose-Einstein condensation temperature $T_\lambda \approx 2.18$ K, liquid ^{4}He begins to gain a component that can be modeled as a quantum inviscid superfluid [1,2]. At intermediate temperatures below T_λ the relative concentrations of normal fluid and superfluid components change in favor of the superfluid component until eventually at sufficiently low temperature ^{4}He becomes inviscid. In addition to the inviscid nature of the superfluid, the vorticity is then carried by vortex-line singularities of fixed circulation $\kappa = h/M$, where h is Planck's constant and M is the mass of the ^{4}He atom [3]. These vortex lines have a core radius $a_0 \approx 10^{-8}$ cm, comparable to the interatomic distance. In generic turbulent state, these vortex lines appear as a complex tangle with a typical intervortex distance $\ell \sim 10^{-4}$–10^{-2} cm [4]. As long as the superfluid component coexists with a normal (viscous) fluid component, the large-scale (much larger than ℓ) hydrodynamic properties of ^{4}He are well described by the well-known two-fluid model, in which the two said components are coupled to each other. The coupling is modeled by the so-called "mutual friction force," which is mediated by the tangle of quantized vortices [2,4–7].

The aim of the present paper is to point out an important difference between classical and quantum turbulent flows. The hydrodynamics of classical fluids is described by the Navier-Stokes equations, in which the viscosity term is responsible for two different physical phenomena. The first is the damping of the kinetic energy of the flow, and it operates also in homogeneous isotropic flows. The second is a crucial ingredient of wall-bounded flows, in which the friction between fluid layers with different *mean* velocities leads to the transfer of linear momentum toward regions with smaller mean velocity [8,9]. The presence of an inviscid superfluid component in quantum turbulence requires a new outlook on these related but distinct phenomena. It was understood that energy dissipation in the superfluid case is caused fundamentally by the existence of the tangle of quantized vortex lines. The work of Vinen and Niemela [4] and later studies [10–13] showed that the rate of kinetic energy dissipation can be modeled well by the introduction of an effective "energy" viscosity, which is traditionally denoted as ν'.

Of course, also superfluid turbulence is usually neither homogeneous nor isotropic, being wall bounded as well. The superfluid velocity fluctuations caused by the dynamics of the tangle of quantized vortices lead to a momentum flux towards the wall. We show here that this momentum transfer can be well modeled by the introduction of a second effective "momentum" viscosity $\nu_{\rm m}$, different from the effective energy viscosity ν'. In particular, we show that the two viscosities have different temperature dependence. The nature of the second effective viscosity is clarified in this paper using two parallel strategies. The first is analogous to classical hydrodynamics requiring the analysis of the Reynolds-stress tensor, which in the present case is determined by the velocity fluctuations created by the quasirandom vortex tangle. The second strategy is in line with the current description of quantum turbulence, using the notion of the "vortex tension force" in the presence of the vortex tangle. We demonstrate that these two strategies lead to the same result. The vortex-tension force, which is current in the superfluid turbulence literature, is analogous to the gradient of the Reynolds-stress tensor, which is more familiar in the classical turbulence literature.

In Sec. II we introduce the notion of the effective momentum viscosity and propose a closure to estimate it in terms of fundamental quantities. Since closure procedures are never rigorous, we present in Sec. III numerical simulations to support and confirm the predictions of the previous section. The concept of "vortex tension force" is explained in Sec. IV, where it is shown that it is understandable as the gradient of the Reynolds stress that is caused by the quantized vortex tangle. The presented analysis is supported again by numerical simulations. Finally, in Sec. V we offer a summary and conclusions.

II. VISCOSITY AND THE TURBULENT MOMENTUM FLUX

A. Reminder from classical turbulence

Consider a classical turbulent fluid flow in a channel geometry with the mean velocity in the $\hat{\boldsymbol{x}}$ direction and with $\hat{\boldsymbol{y}}$ being the wall-normal direction. The fluid velocity field can be decomposed into the mean velocity $\boldsymbol{V}(y)$ plus

turbulent velocity fluctuations $\tilde{\boldsymbol{v}}$. The mean velocity has only one component $V_x(y)$ such that

$$\boldsymbol{v}(\boldsymbol{r}) = \hat{\boldsymbol{x}}\, V_x(y) + \tilde{\boldsymbol{v}}(\boldsymbol{r}). \tag{1}$$

Then the continuity equation for the x projection of the mean linear mechanical momentum density per unit mass [which is exactly $V_x(y)$] can be written as

$$\frac{\partial V_x}{\partial t} + \frac{\partial\, \Pi_{xy}}{\partial y} = 0, \tag{2a}$$

where the momentum flux towards the wall Π_{xy} is given exactly by the sum of two contributions, the mean shear $S(y)$ and the so-called Reynolds stress $W(y)$,

$$\Pi_{xy}(y) = \nu\, S(y) + W(y),$$
$$S(y) = \frac{\partial V_x}{\partial y}, \quad W(y) = \langle \widetilde{v}_x \widetilde{v}_y \rangle. \tag{2b}$$

Here ν is the kinematic viscosity of the fluid and $\langle \cdots \rangle$ stands for the appropriate average (either over time or over an ensemble). This is as far as one can go exactly. To estimate the Reynolds stress we follow, an old idea of Boussinesq [14], who suggested that in wall-bounded flows $W(y) \propto S(y)$,

$$\langle \widetilde{v}_x \widetilde{v}_y \rangle \simeq \nu_{\text{T}} S(y), \tag{3}$$

where ν_{T} is an effective "turbulent" viscosity that needs to be estimated as a product of a typical length scale and a typical velocity scale:

$$\nu_{\text{T}} \simeq l_{\text{ch}} v_{\text{ch}}. \tag{4}$$

The typical velocity scale is estimated as a square root of the kinetic energy density per unit mass, $K(y) = \langle |\tilde{\boldsymbol{v}}(\boldsymbol{r})|^2 \rangle/2$. The typical length scale in wall-bounded flows is the distance to the wall, denoted here as y. We thus end up with the estimate

$$\nu_{\text{T}} \approx y\sqrt{K(y)}, \quad W(y) \approx y\sqrt{K(y)}S(y), \tag{5}$$

up to constants of the order of unity.

B. The case of quantum turbulence

Consider next a superfluid flowing in the same channel configuration and explore the necessary modifications of the continuity Eq. (2) for the density of the mechanical momentum of superfluid, in which the momentum flux now takes the form

$$\Pi_{xy,s} = W_{\text{s}}(y) + \mathcal{F}_{\text{mf}}(y), \quad W_{\text{s}}(y) = \langle \widetilde{v}_{x,\text{s}}\, \widetilde{v}_{y,\text{s}} \rangle. \tag{6}$$

Here $\widetilde{\boldsymbol{v}}_{\text{s}}$ are the superfluid velocity fluctuations caused by fluctuating vortex lines. The "appropriate average" $\langle \cdots \rangle$ now means averaging over the vortex tangle in a "physically small volume," which should include vortex lines which are much longer than the intervortex spacing, but short enough compared to the characteristic scale on the problem. In our particular geometry we choose this volume as a slice between y and $y + \delta y$, going over all x and z, with δy much smaller than the channel half-width H. In this paper we consider only stationary turbulence. This allows us to improve statistics by additional averaging over time. In other words, hereafter by $\langle \cdots \rangle$ we mean $\langle \cdots \rangle_{x,z,t}$.

For the inviscid component the viscosity is zero, and in Eq. (6) there is no explicit shear term $\nu S(y)$ in the momentum flux. Instead there is a contribution from the mutual friction force $\mathcal{F}_{\text{mf}}(y)$, which is not discussed in this paper. What is important for us here is that the Reynolds stress, however, still contribute to Eq. (6), but now correlating the fluctuations of the velocity of the superfluid. We propose that Eqs. (3) and (4) are still appropriate, except that in the case of superfluids with random vortex tangles there is another characteristic length besides the distance to the wall. This length is the mean intervortex distance $\ell(y)$, which we propose to take as the estimate of l_{ch} in Eq. (3),

$$l_{\text{ch}} \approx \ell(y), \quad \ell(y) = 1/\sqrt{\mathcal{L}}(y), \tag{7}$$

again up to constants of the order of unity. Here $\mathcal{L}(y)$ is the vortex-line density, i.e., the vortex-line length per unit volume. Notice that in all our calculations and discussions we assume that the vortex tangle is dense enough, such that $\mathcal{L}(\boldsymbol{r})$ is a well-defined, smooth macroscopic field.

The characteristic velocity scale should be again provided by the square-root of a kinetic energy density, but the appropriate one in this case is the kinetic energy density K of the random vortex tangle. To connect this energy density to the vortex-line density, we follow Feynman [3], who related the kinetic energy density to the vortex-line density as $K \simeq \kappa^2\, \mathcal{L}$. For quantum turbulence which is weakly varying in space at distances $\sim\ell$ it is tempting to assume that this estimate is satisfied locally,

$$K(y) \approx \kappa^2 \mathcal{L}(y), \quad \Rightarrow \sqrt{K(y)} \approx \kappa/\ell(y), \tag{8}$$

up to constants of the order of unity. The upshot of this discussion is that for wall-bounded superfluid turbulence we can estimate the superfluid Reynolds stress as

$$W_s(y) = \nu_{\text{m}}\, S(y), \quad \nu_{\text{m}} \approx \kappa. \tag{9}$$

Here ν_{m} is an effective "momentum" kinematic viscosity and $S(y)$ is given by Eq. (2), in which now V_x is the mean superfluid velocity in the streamwise direction x, $V_{x,\text{s}}$. Henceforth, we omit subscript s from the quantities related to the superfluid.

The conclusion is therefore as follows: The contribution to the momentum flux towards the wall, which is carried by the superfluid turbulent velocity fluctuations, is determined by an effective momentum viscosity of the order of the quantum circulation κ and is independent of the vortex-line density profile.

Notice that another parameter in the problem of the dynamics of superfluid turbulence has the same dimensionality: the diffusion coefficient of the inhomogeneous vortex tangle. The diffusion of the inhomogeneous tangle was studied by Tsubota, Araki, and Vinen [15] and by Nemirovskii [16] and the diffusion coefficient D was estimated to be of the order of 0.1κ in [15] and of $\approx 2.2\kappa$ in [16]. Nemirovskii and Tsubota in [17] also studied dynamics of the Lamb impulse $\boldsymbol{J} \propto \int \boldsymbol{r} \times \boldsymbol{\omega}(\boldsymbol{r})\, d\boldsymbol{r}$ that sometimes is used to replace mechanical momentum. Nevertheless, the Lamb impulse is not exactly conserved in superfluid turbulence [17] and therefore will not be involved in our studies.

Obviously, the derivation of Eq. (9) for ν_{m} is not rigorous, and it requires an experimental verification. Unfortunately, there are no experimental studies allowing us at present to clarify to which degree this simple prediction corresponds to

physical reality. We are therefore forced at the present time to test the prediction with numerical simulations.

III. NUMERICAL SIMULATIONS

A. Preparation of the system

To test our ideas, we performed numerical simulations of quantized vortex-line dynamics in a three-dimensional planar channel geometry $L_x \times L_y \times L_z$ of half-width H, $L_x = 4H$, $L_y = 2H$, $L_z = 2H$, $H = 0.05$ cm (Fig. 1). To force turbulence, we use prescribed a time-independent profile of the streamwise projection of the normal velocity $V_{x,\mathrm{n}}(y) \equiv V_\mathrm{n}(y)$. To find the resulting vortex tangle configurations, we used the vortex filament method [18], taking into account the potential flow to maintain the counterflow condition.

More details of the simulation method can be found in Refs. [19,20]. Here we used the reconnection method [21] and the line resolution $\Delta\xi = 1.6\times10^{-3}$ cm. Periodic conditions were used in the streamwise and spanwise directions. Taking into account the fact that the boundary conditions for the superfluid component are still under discussion, we adopted their simplest version: In the wall-normal y direction $V_y(\pm H) = 0$ and $\boldsymbol{s}'(\pm H) = (0, \pm 1, 0)$ at the solid walls.

Having selected a stationary profile of $V_\mathrm{n}(y)$, we initiated the simulations with a set of arbitrary oriented circular vortex rings and solved the equations for the vortex-line evolution. Given the resulting dense vortex tangle, we found the profiles of all quantities of interest by averaging over periodic directions and over time for 20 s of steady-state evolution. To find $W(y)$, we have calculated the superfluid velocity field $\boldsymbol{v}(\boldsymbol{r},t)$ on a $128\times64\times128$ grid and then determined the profile $W(y) = \langle v_x v_y\rangle - V_x V_y$. Similarly, the turbulent kinetic energy profile was computed from $2K(y) = \langle \boldsymbol{v}^2\rangle - V_x^2$. The details of the calculation of the Reynolds-stress tensor from the structure of the vortex tangle are given in Appendix A.

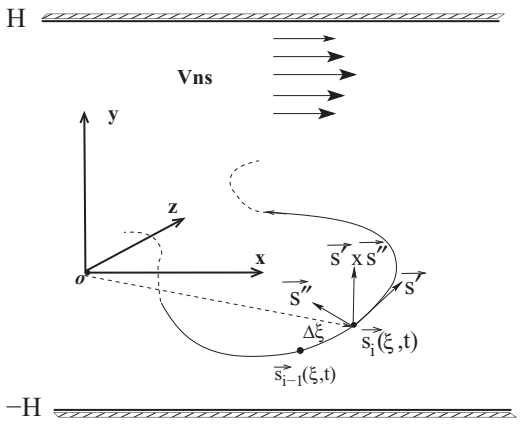

FIG. 1. The Cartesian coordinates and the local vortex-line parametrization in a plane channel flow geometry. The counterflow velocity $\boldsymbol{V}_\mathrm{ns} = \boldsymbol{V}_\mathrm{n} - \boldsymbol{V}_\mathrm{s}$ is oriented along the positive streamwise direction. Here $\boldsymbol{s}(\xi)$ are the Cartesian coordinates of the vortex-line point. The vortex line is parametrized by the arclength ξ. The derivative $\boldsymbol{s}' = d\boldsymbol{s}/d\xi$ is a unit vector in the direction of the vortex line; $\boldsymbol{s}'' = d^2\boldsymbol{s}/d\xi^2$ is a vector normal to the vortex line with the norm equal to its local curvature.

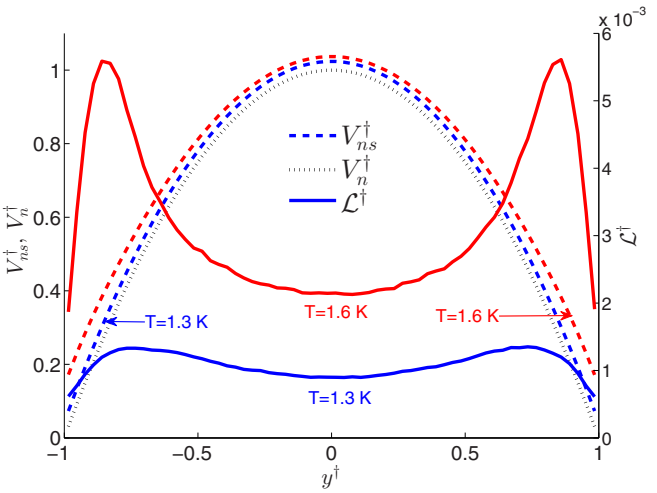

FIG. 2. Prescribed parabolic normal velocity profile $V_\mathrm{n}^\dagger(y^\dagger)$ (black dotted line), the resulting profiles of the counterflow velocity $V_\mathrm{ns}^\dagger(y^\dagger)$ (dashed lines), and the vortex-line density $\mathcal{L}^\dagger(y^\dagger)$ (solid lines). Blue lines show data for $T = 1.3$ K; red lines show data for $T = 1.6$ K. For both temperatures the centerline normal fluid velocity $V_\mathrm{n}(0) = 1.2$ cm/s.

Before presenting the results of the simulations we stress that the suggested closure for the Reynolds stress in the quantum turbulence case was based on an analogy with classical turbulence. It does not account for the two-fluid character of superfluid ^{4}He at intermediate temperatures. Therefore, we cannot expect this closure to be optimal at temperatures for which the normal fluid and superfluid densities are comparable. Accordingly, we focus here on the low-temperature regime. For $T = 1.3$ K and 1.6 K the normal fluid densities are $\rho_\mathrm{n}/\rho \approx 0.045$ and 0.162, respectively [1]. A control test with $T = 1.9$ K, when $\rho_\mathrm{n}/\rho \approx 0.42$, is shortly discussed later. At each temperature we tested three different values of the centerline counterflow velocity corresponding to the mean vortex-line densities in the interval $(2\text{–}8)\times10^3$ cm^{-2} (see Fig. 4). The results are presented in dimensionless units with the following normalizations:

$$y^\dagger = y/L, \quad V^\dagger = V/V_\mathrm{n}(0), \quad \mathcal{L}^\dagger(y) = \kappa^2\mathcal{L}/[V_\mathrm{n}(0)]^2,$$
$$K^\dagger(y) = 2K(y)/[V_\mathrm{n}(0)]^2, \quad W^\dagger(y) = W(y)/[V_\mathrm{n}(0)]^2.$$

In Fig. 2 we show by a black dotted line the prescribed parabolic profile of the normal velocity (identical for the two featured temperatures) and by blue and red dashed lines the resulting mean counterflow velocity profiles (for $T = 1.3$ K and 1.6 K, respectively). At these temperatures the normal-fluid density ρ_n is much smaller than ρ_s. The condition of net mass flow $\rho_\mathrm{n}\langle V_\mathrm{n}(y)\rangle_y + \rho_\mathrm{s}\langle V(y)\rangle_y = 0$ implies that $|\langle V_\mathrm{n}(y)\rangle_y| \gg |\langle V(y)\rangle_y|$. Here $\langle\cdots\rangle_y$ denotes averaging over the wall-normal direction y. Accordingly, the counterflow velocity profiles $V_\mathrm{ns}(y) = V_\mathrm{n}(y) - V(y)$ in Fig. 2 are not very different from the prescribed profile $V_\mathrm{n}(y)$.

Notice that the profiles of the vortex-line density $\mathcal{L}(y)$ and the counterflow velocity $V_\mathrm{ns}(y)$ are very different. In fact, the vortex lines tend to concentrate in regions with weaker counterflow velocity. Therefore, the famous relation [7] between the mean vortex-line density and the mean counterflow velocity

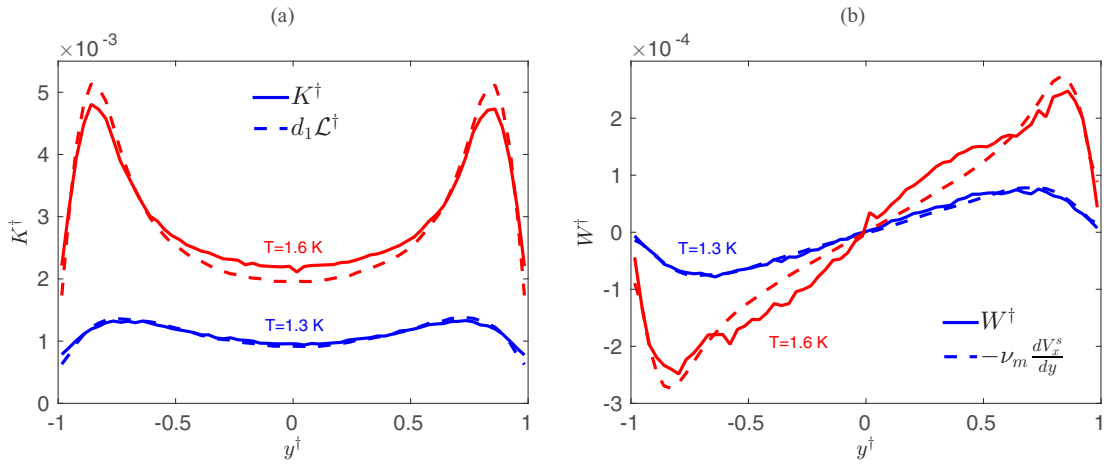

FIG. 3. Verification of the closure for the effective momentum viscosity. (a) Comparison of the turbulent kinetic energy profiles $K^\dagger(y)$ (solid lines) with the vortex-line density $d_1\mathcal{L}^\dagger(y)$ (dashed lines). Here d_1 is a constant of the order of unity. (b) Comparison of the Reynolds-stress profiles $W^\dagger$ (solid lines) and the normalized shear profiles $-\nu_{\rm m}S^\dagger$ (dashed lines). $T = 1.3$ K (blue lines) and $T = 1.6$ K (red lines). For both temperatures $V_{\rm n}(0) = 1.2$ cm/s. Both parameters (d_1 and $\nu_{\rm m}$) were obtained by best fit.

$\mathcal{L} \propto V_{\rm ns}^2$ holds only globally and is not fulfilled locally across the channel.

B. Confirmation of the concept of $\nu_{\rm m}$

To test (and confirm) the suggested closure (9), we demonstrate in Fig. 3(a) that the profile of the turbulent kinetic energy $K(y)$ is indeed proportional to the vortex-line density profile, as required by Eq. (8) that leads to the closure (9). Indeed, there is an excellent correspondence between $K(y)$ and $\mathcal{L}(y)$ profiles for $T = 1.3$ K (blue lines), with only a slight discrepancy between them for $T = 1.6$ K (red lines). Even for $T = 1.9$ K (not shown) the agreement between $K(y)$ and $\mathcal{L}(y)$ is fairly good.

Next we compared in Fig. 3(b) the profiles of the Reynolds stress $W^\dagger(y)$ with the normalized shear profile $[\nu_{\rm m}S]^\dagger(y) = -\nu_{\rm m}[dV(y)/dy]/[V_{\rm n}(0)]^2$. The closure approximation $[\nu_{\rm m}S]^\dagger(y^\dagger)$ follows closely the behavior of $W^\dagger(y^\dagger)$: Notice the (almost) linear profile in the center of channel and the drop near the wall. Similarly to the kinetic energy, there is an excellent correspondence between $W^\dagger(y^\dagger)$ and $[\nu_{\rm m}S]^\dagger(y\dagger)$ profiles for $T = 1.3$ K (blue lines) and some slight deviations between them for $T = 1.6$ K (red lines). For a higher temperature $T = 1.9$ K (not shown) the closure $[\nu_{\rm m}S]^\dagger(y^\dagger)$ reproduces $W^\dagger(y^\dagger)$ only qualitatively. We conjecture that this is due to the influence of the normal fluid component which is not accounted for in the closure.

The comparison of the numerically found profiles $W(y)$ and $\nu_{\rm m}S(y)$ allows us to measure the effective momentum viscosity ν_m. Its temperature and mean-vortex line density $\langle\mathcal{L}\rangle$ dependence is shown in Fig. 4. The viscosity $\nu_{\rm m}(T, \langle\mathcal{L}\rangle)$ decreases upon increasing either the temperature or the vortex-line density. Notice that the temperature dependence of $\nu_{\rm m}(T)$ is opposite to that of the Vinen effective energy viscosity $\nu_{\rm e}(T)$, which increases with temperature. We stress here that Eq. (9) predicts that $\nu_{\rm m}$ is constant across the channel, which is confirmed by Fig. 3(b). Its dependence on mean vortex-line density may come from different $\mathcal{L}$ dependencies of the Reynolds stress and the shear. The study of this dependence is beyond the scope of this paper.

IV. REYNOLDS STRESS GRADIENT AND VORTEX-TENSION FORCE

A. Analysis

The idea of taking into account the effect of the small-scale structures of the quantum vortex tangle on the macroscopic equations of motion is not new. In 1958 Hall [5] introduced the concept of the tension force $\boldsymbol{T}$ (caused by a Magnus effect) that acts on the curved vortex line moving through the liquid. Accounting for the Bernoulli pressure drop over the surface of a tube around the vortex, Hall found an expression for $\boldsymbol{T}$ (denoted below as $\boldsymbol{T}_{\rm H}$), acting on the vortex line, which in our notations reads

$$\boldsymbol{T}_{\rm H} = -\frac{\kappa^2\Lambda}{4\pi}\,\boldsymbol{s}'', \quad \Lambda = \ln\frac{\ell}{a_0}. \tag{10a}$$

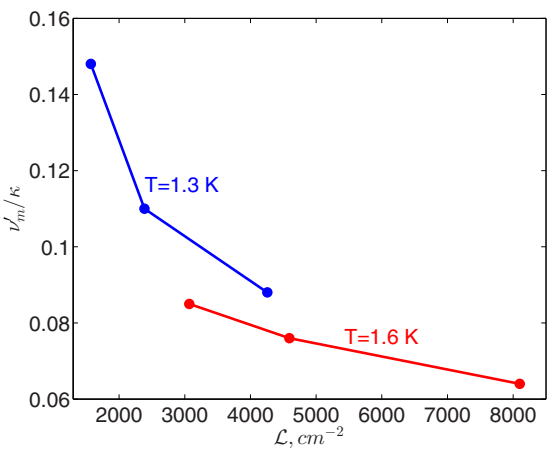

FIG. 4. The temperature and the vortex-line density dependence of the effective momentum viscosity $\nu_{\rm m}/\kappa$.

Recall that $\boldsymbol{s}'' = d^2\boldsymbol{s}/d\xi^2$ is a vector normal to the vortex line with a norm equal to its local curvature. Averaging Hall's result (10a) over the vortex tangle configuration in a slice of width $\ell \ll \delta \ll H$ around a given y and going over all x and z gives

$$\boldsymbol{\mathcal{T}}_{\rm H}(y) = -\frac{\kappa^2\Lambda}{4\pi}\,\langle \boldsymbol{s}''\rangle \mathcal{L}(y). \tag{10b}$$

In this section we show that the mean gradient of the Reynolds-stress tensor, $\langle(\widetilde{\boldsymbol{v}}\cdot\boldsymbol{\nabla})\widetilde{\boldsymbol{v}}\rangle$, calculated under the simplifying assumption that the fluctuating part of the velocity is produced by a local velocity close to the vortex lines, coincides with the tension force.

To this end consider first the velocity close to the vortex line [22],

$$\widetilde{\boldsymbol{v}}(\boldsymbol{R}) = \frac{\kappa}{2\pi R^2}[X(\boldsymbol{s}'\times\boldsymbol{s}'') - Y\boldsymbol{s}'']\left(\frac{1}{|\boldsymbol{s}''|}+\frac{X}{2}\right) + \frac{\kappa(\Lambda-1)}{4\pi}\boldsymbol{s}'\times\boldsymbol{s}'', \tag{11}$$

where (X,Y) are the local Cartesian coordinates, associated with the line point and $R^2 = X^2+Y^2$. We then substitute this velocity into $(\widetilde{\boldsymbol{v}}\cdot\boldsymbol{\nabla})\widetilde{\boldsymbol{v}}$. After some cumbersome calculations, detailed in Appendix B, we get for the mean gradient of the Reynolds-stress tensor:

$$\left\langle(\widetilde{\boldsymbol{v}}\cdot\boldsymbol{\nabla})\widetilde{\boldsymbol{v}}\right\rangle = -\frac{\kappa^2\Lambda}{8\pi}\,\langle \boldsymbol{s}''\rangle \mathcal{L}(y). \tag{12}$$

The right-hand side (RHS) of this equation differs from Eq. (10b) for the tension force only by a factor of two. A possible origin of this factor is an inconsistent expansion of the velocity near the vortex line in the derivation of $\boldsymbol{T}$ in [5], which was not given explicitly.

Based on the similarity of the RHSs of Eqs. (10b) and (12), we suggest for the vortex-tension force the following expression in terms of the tangle configuration:

$$\boldsymbol{\mathcal{T}}(y) = -\frac{\kappa^2\Lambda}{8\pi}\,\langle \boldsymbol{s}''\rangle \mathcal{L}(y). \tag{13}$$

The upshot of this calculation is that the gradient of the Reynolds-stress tensor of velocity fluctuations $\langle(\widetilde{\boldsymbol{v}}\cdot\boldsymbol{\nabla})\widetilde{\boldsymbol{v}}\rangle$ on the scale of the intervortex distance and the tension force $\boldsymbol{\mathcal{T}}$, given by the right-hand side of Eq. (12) are actually the same. The tension force was derived and used in the context of quantum turbulence; the Reynolds-stress tensor is more familiar in the context of classical turbulence. We can summarize the consequences of this identity, using Eqs. (2b), (9), and (12) to provide a remarkably simple representation of Eq. (13) for the tension force via the mean superfluid velocity $\boldsymbol{V}(\boldsymbol{r})$:

$$\boldsymbol{\mathcal{T}}(\boldsymbol{r}) = \nu_{\rm m}\Delta\boldsymbol{V}(\boldsymbol{r}). \tag{14}$$

We believe that this new interpretation carries an important advantage. In the original Eq. (13) the tension force $\boldsymbol{\mathcal{T}}$ is dominated by the small-scale ($\sim\ell$) structure of the vortex tangle, which is very difficult to find analytically. On the other hand, in the closure approximation (14) the main contribution to the mean velocity $\boldsymbol{V}(\boldsymbol{r})$ comes from the largest scales in the flow. This would allow a regular description as modeled in classical wall-bounded turbulence [9].

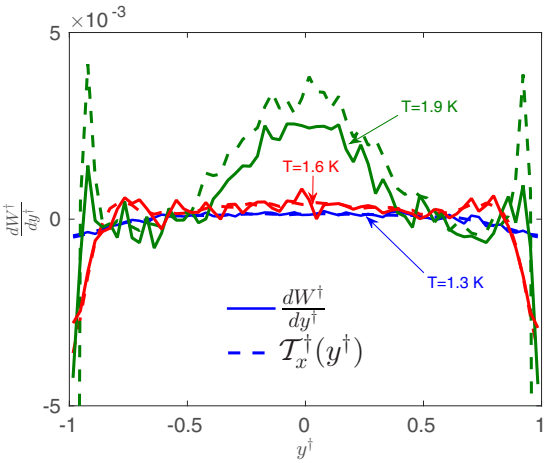

FIG. 5. Comparison of the numerical results for the gradient of the Reynolds stress $\partial\langle\widetilde{v}_x\,\widetilde{v}_y\rangle/\partial y$ (solid lines), computed via fluctuating velocity field, and the streamwise projection of the tension force $\mathcal{T}_x(y)$ (dashed lines), found from the vortex configuration by (13). Temperatures $T = 1.3$ K, $T = 1.6$ K, and $T = 1.9$ K. $V_{\rm n}(0) = 1.2$ cm/s.

B. Numerical confirmation

Equation (12) was derived on the basis of the approximation that the fluctuating part of velocity is given by the local velocity in the proximity of the vortex line. Larger-scale fluctuations were neglected. We therefore need to test the approximation using our simulations. The justification of the approximation is shown in Fig. 5, where the numerical results for the gradient of the Reynolds stress, $\partial\langle\widetilde{v}_x\,\widetilde{v}_y\rangle/\partial y$, computed via fluctuations of the velocity field, are shown by solid lines, while the $\mathcal{T}_x(y)$ (the only nonzero component of the tension force in our geometry), calculated by Eq. (13) from the vortex-line configurations, is plotted by dashed lines. Clearly, these lines practically coincide (up to numerical noise), without any fitting parameters, for all the studied temperatures, including $T = 1.9$ K.

We conclude that our analytical and numerical results demonstrate that the gradient of the Reynolds stress and the tension force, both originated from the motions of the random vortex tangle, are identical objects.

V. SUMMARY AND THE ROAD AHEAD

In superfluid turbulence there are two related phenomena that stem from the existence of a tangle of quantized vortices. Although the intervortex distance ℓ is small, the effect of the vortex tangle appears also in the dynamics of large scales. One effect is the Vinen effective viscosity ν', which describes the rate of energy dissipation. In this paper we introduced a second effective viscosity $\nu_{\rm m}(T)$ that describes the transfer of linear mechanical momentum toward regions with lower mean velocity. It appears in the friction force $\nu_{\rm m}(T)\Delta\boldsymbol{V}(\boldsymbol{r},t)$. This friction force operates between layers with different superfluid velocities $\boldsymbol{V}(\boldsymbol{r},t)$, mediated by the random vortex tangle.

The second result of this paper follows from an analysis of the gradient of the vortex tangle-induced Reynolds-stress tensor and of the vortex-tension force $\boldsymbol{\mathcal{T}}$. We show that these

two objects are just different names for the same mechanism of transfer of linear mechanical momentum.

Additional analysis is required to fully understand the properties of the effective momentum viscosity $\nu_{\rm m}(T)$ and to clarify its range of applicability. These subjects go beyond the scope of this paper and will be dealt with in future publications.

APPENDIX A: NUMERICAL CALCULATIONS OF REYNOLDS-STRESS TENSOR

The numerical integration for Reynolds-stress tensor was done on the grid of $128\times64\times128$ points. At each grid point the velocity induced by the entire vortex tangle was calculated. Understanding that velocity close to the vortex line depends on r as $1/r$, we expect that $v_i v_j \sim 1/r^2$ and therefore regions close to the vortex lines could have large contribution to the $\langle v_i v_j\rangle$. On the other hand, at our limited resolution in the vortex-line evolution, we do not expect to properly describe the velocity very close to the vortex line. To control the calculation of the velocity, we use the following procedure. While calculating the contribution of line segment to the velocity at a particular grid point, we measured the shortest distance between this grid point and the line segment. If this distance was smaller than some critical distance $\delta_{\rm cr}$, we set this distance to be equal to $\delta_{\rm cr}$. The critical distance $\delta_{\rm cr}$ was chosen to be much smaller than size of the grid, such that this procedure significantly affected only contribution from the closest vortex segment, but not too small, such that the contribution of this segment to the velocity may be considered as reliable. We repeated this procedure for different values of $\delta_{\rm cr}$, ranging from $\delta_{\rm cr}=0.1$ μm to $\delta_{\rm cr}=1$ μm (for comparison, the distance between grid points in the y direction is 15.6 μm and the average interpoint distance in the vortex tangle is 16 μm). We have found that the profiles of the kinetic energy and the Reynolds stress for $\delta_{\rm cr}=0.3$ μm were smooth and the contributions of the line segments close to the grid points (about 10% of the segments in each configuration) did not overshadow the contributions from the rest of the tangle. For smaller $\delta_{\rm cr}$ the contributions from just few segments close to grid points dominated the velocity at the corresponding grid point, making the profiles not well defined. The results of the present paper correspond to $\delta_{\rm cr}=0.3$ μm. The values of K and W have grown by about 10% in going from $\delta_{\rm cr}=1$ μm to $\delta_{\rm cr}=0.3$ μm, retaining the shape of the profile. We thus consider our results as a low bound for the profiles of the kinetic energy and the Reynolds stress.

APPENDIX B: CALCULATION OF REYNOLDS STRESS VIA VORTEX CONFIGURATION

In order to calculate $\langle(\widetilde{\boldsymbol{v}}\cdot\boldsymbol{\nabla})\widetilde{\boldsymbol{v}}\rangle$ in terms of the vortex-tangle configuration, we recall that this averaging includes integration of the vortex configuration over a slice of width $\ell\ll\delta y\ll H$ going over all x and z. Keeping in mind that the main contribution to this integral comes from the areas close to the vortex lines, we start by writing explicitly the contributions to the velocity close to the vortex line given by Eq. (11):

$$v_{\rm X}=\frac{\kappa}{4\pi}\left[-\frac{2Y}{R^2}-\frac{XY}{R^2}|s''|\right],$$
$$v_{\rm Y}=\frac{\kappa}{4\pi}\left[\frac{2X}{R^2}-\frac{Y^2}{R^2}|s''|+|s''|\Lambda\right]. \tag{B1}$$

These expressions were obtained as a consistent first-order expansion in curvature $|s''|$.

Next we calculate the derivatives of the velocities with respect to local coordinates X and Y:

$$\frac{\partial v_{\rm X}}{\partial X}=\frac{\kappa}{2\pi}\left[\frac{2XY}{R^4}-\frac{Y}{2R^2}|s''|+\frac{X^2Y}{R^4}|s''|\right],$$
$$\frac{\partial v_{\rm X}}{\partial Y}=\frac{\kappa}{2\pi}\left[-\frac{1}{R^2}+\frac{2Y^2}{R^4}-\frac{X}{2R^2}|s''|+\frac{XY^2}{R^4}|s''|\right],$$
$$\frac{\partial v_{\rm Y}}{\partial X}=\frac{\kappa}{2\pi}\left[\frac{1}{R^2}-\frac{2X^2}{R^4}+\frac{Y^2X}{R^4}|s''|-\frac{X}{2R^2}|s''|\right],$$
$$\frac{\partial v_{\rm Y}}{\partial Y}=\frac{\kappa}{2\pi}\left[-\frac{2YX}{R^4}-\frac{Y}{R^2}|s''|+\frac{Y^3}{R^4}|s''|-\frac{Y}{2R^2}|s''|\right]. \tag{B2}$$

It is customary to perform the integration of the velocity close to the vortex line using a curvilinear coordinate system associated with a vortex line, in which the first coordinate is the arclength ξ and the other two are the polar coordinates in the plane perpendicular to $\boldsymbol{s}'$ with a polar axis that form an angle $\psi(\xi)$ with $\boldsymbol{s}''$. Here $\psi(\xi)$ is defined via torsion of the vortex line τ as $\tau=d\psi(\xi)/d\xi$.

The coordinate system, defined in this way, is orthogonal with metric coefficients [22],

$$h_\theta=R;\quad h_R=1;\quad h_\xi=1-R|s''|\cos(\theta-\psi), \tag{B3}$$

where θ is an azimuthal angle in the polar plane.

Then the relation between Cartesian and polar coordinates is given by $X=R\cos(\theta-\psi)$, $Y=R\sin(\theta-\psi)$, such that the element of volume is

$$d\Omega=R[1-R|s''|\cos(\theta-\psi)]dRd\theta d\xi. \tag{B4}$$

Now, substituting Eqs. (B1) and (B2) into $(\widetilde{\boldsymbol{v}}\cdot\boldsymbol{\nabla}\widetilde{\boldsymbol{v}})$ and integrating in the cylindrical volume around vortex line and afterwards integrating along the vortex lines $\mathcal{C}'$ in the slice, after some algebra we get

$$\frac{1}{\Omega}\int(\widetilde{\boldsymbol{v}}\cdot\boldsymbol{\nabla})\widetilde{\boldsymbol{v}}d\Omega=-\frac{\kappa}{8\pi\Omega_{\mathcal{C}'}}\int_{\mathcal{C}'}\boldsymbol{s}''d\xi\int_{a_0}^{\ell}\frac{dR}{R}=-\frac{\kappa\langle\boldsymbol{s}''\rangle}{8\pi}\Lambda\mathcal{L}, \tag{B5}$$

where $\Omega_{\mathcal{C}'}=4H^2\delta y$ is the slice volume.

[1] R. J. Donnelly and C. F. Barenghi, J. Phys. Chem. Ref. Data **27**, 1217 (1998).

[2] R. J. Donnelly, *Quantized Vortices in Hellium II* (Cambridge University Press, Cambridge, 1991).

[3] R. P. Feynman, Prog. Low Temp. Phys. **1**, 17 (1955).

[4] W. F. Vinen and J. J. Niemela, J. Low Temp. Phys. **128**, 167 (2002).

[5] H. E. Hall, Proc. R. Soc. Lond. A **245**, 546 (1958).

[6] H. E. Hall and W. F. Vinen, Proc. R. Soc. Lond. A **238**, 215 (1956).

[7] W. F. Vinen, Proc. R. Soc. Lond. A **243**, 400 (1958).
[8] U. Frisch, *Turbulence: The Legacy of A. N. Kolmogorov* (Cambridge University Press, Cambridge, 1995).
[9] S. B. Pope, *Turbulent Flows* (Cambridge University Press, Cambridge, 2000).
[10] W. F. Vinen, J. Low Temp. Phys. **161**, 419 (2010).
[11] L. Skrbek and K. R. Sreenivasan, Phys. Fluids **24**, 011301 (2012).
[12] S. Nemirovskii, Phys. Rep. **524**, 85 (2013).
[13] L. Boue, V. S. L'vov, Y. Nagar, S. V. Nazarenko, A. Pomyalov, and I. Procaccia, Phys. Rev. B **91**, 144501 (2015).
[14] J. Boussinesq, *Theorie de làcoulement tourbillant* (Mem. Pres. Acad. Sci., Paris, 1877), Vol. XXIII, p. 46.
[15] M. Tsubota, T. Araki, and W. F. Vinen, Physica B **329**, 224 (2003).
[16] S. K. Nemirovskii, Phys. Rev. B **81**, 064512 (2010).
[17] S. Nemirovskii and M. Tsubota, J. Low Temp. Phys. **113**, 591 (1998).
[18] K. W. Schwarz, Phys. Rev. B **38**, 2398 (1988).
[19] L. Kondaurova, V. S. L'vov, A. Pomyalov, and I. Procaccia, Phys. Rev. B **89**, 014502 (2014).
[20] D. Khomenko, L. Kondaurova, V. S. L'vov, P. Mishra, A. Pomyalov, and I. Procaccia, Phys. Rev. B **91**, 180504(R) (2015).
[21] D. C. Samuels, Phys. Rev. B **46**, 11714 (1992).
[22] P. G. Saffman, *Vortex Dynamics* (Cambridge University Press, Cambridge, 1992).